International Journal of Material Forming (2022) 15: 12
https://doi.org/10.1007/s12289-022-01651-1

DEVELOPMENTS IN MODELLING AND SIMULATION..JAPAN, SOUTH KOREA AND CHINA

Description of elastic–plastic stress–strain transition in cyclic plasticity and its effect on springback prediction

Fusahito Yoshida[1,2]

Received: 6 September 2021 / Accepted: 10 January 2022 / Published online: 14 February 2022

Abstract
In the cyclic plasticity deformation of metallic materials, nonlinear elastic unloading and subsequent smooth elastic–plastic stress–strain behavior is observed in reverse loading owing to the Bauschinger effect. To determine how accurately material models can describe the elastic–plastic transition behavior, cyclic stress–strain simulations were conducted and their results were compared with the corresponding results for DP980 and 590R high-strength steel (HSS) sheets. The two plasticity models, the Yoshida–Uemori (Y-U) pure kinematic hardening (KH) model and the Armstrong–Frederick KH combined with isotropic hardening (A-F–KH + IH) model, were used with four different types of elasticity models, Young's modulus, plastic-strain-dependent chord modulus, yield-surface-average (YSA) elastic modulus, and nonlinear elastic model. The best model to describe the realistic elastic-plastic transition behavior was the Y-U model combined with the nonlinear elastic model. The effects of these material models on springback prediction were examined based on a plane-strain bending–unbending springback simulation. When using the Y-U model, the amounts of springback and residual stresses calculated by the two plastic-strain–dependent linear elastic models and the nonlinear elastic model were almost the same. By contrast, when using the A-F–KH + IH model, the calculated results using the linear elastic models were quite different from those of the nonlinear model calculation. The effect of the yield plateau on the springback calculation was minor.

Keywords Elastic–plastic transition · Yoshida–Uemori model · Armstrong–Frederick model · plastic-strain-dependent elastic model · springback

Introduction

The use of an appropriate material model of elasto-plasticity is vital for accurate sheet metal forming simulations. Specifically, for springback, the plastic-strain-dependent elastic modulus and the Bauschinger effect are the two most influential unloading properties of materials [1–22]. The amount of springback is determined as a function of the bending moment at the final stage of forming (which is the driving force of springback) and unloading elastic modulus. Furthermore, if re-yielding occurs during unloading owing to the Bauschinger effect, it should be considered for springback simulation. The advanced high-strength steel (AHSS) sheets are prone to springback-induced re-yielding because the bending moment becomes very large because of their high flow stress, and furthermore, they exhibit strong Bauschinger effect.

The unloading elastic modulus is usually measured from the stress–strain slope in the sequential tensile loading–unloading experiment. Although the unloading–reloading stress–strain response after a plastic deformation is slightly curved owing to micro plasticity [1, 2], as shown in Fig. 1**,** the elastic modulus is usually determined from the stress-strain slope from the unloading-start point (point *a* in Fig. 1) to the stress-zero point (point *b* in Fig. 1). Therefore, the obtained elastic modulus is often called "chord modulus", and it decreases remarkably with increasing plastic strain [2, 17, 23–25]. To describe the plastic-strain-dependent elastic modulus degradation, Yoshida et al. [2] proposed the following simple mathematical model:

✉ Fusahito Yoshida
fyoshida@hiroshima-u.ac.jp

[1] Institute of Advanced Science and Engineering, Hiroshima University, Higash-Hiroshima, Japan

[2] CEM Institute Corporation, Higash-Hiroshima, Japan

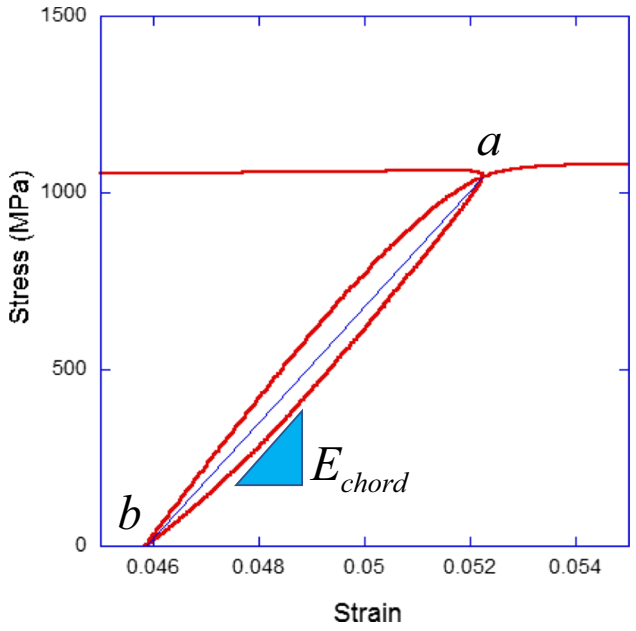

Fig. 1 Nonlinear stress–strain response and chord modulus of elasticity in sequential tension-unloading experiment

$$E = E_{chord} = E_o - \left(E_o - E_a\right)\left[1 - \exp\left(-\xi p\right)\right]. \quad (1)$$

Here, E_o and E_a denote Young's modulus (= elastic modulus of virgin materials) and asymptotic elastic modulus at infinitely large plastic deformation, respectively, and a material parameter, ξ,controls the rate of the elastic modulus degradation. This model is widely used in springback simulation.

In addition to the chord modulus model, which assumes the linear stress–strain response, some elastic models to describe the nonlinear unloading behavior (Fig. 1) have been proposed. Sun and Wagoner [16] proposed the quasi-plastic-elastic (QPE) model, which is the first nonlinear unloading model, wherein the elastic modulus is expressed as a function of elastic and QPE strain accumulation. Several elastic models in the QPE framework were later published [14, 26, 27]. In addition to the QPE-type modeling, Lee J.-Y. [28] proposed a Mróz(1967)-type [29] multi-surface model, and Eggertsen et al. [30] and Sumikawa et al. [21] described the nonlinear unloading stress-strain response as an elasto–plasticity behavior. Although these models successfully describe the nonlinear unloading stress–strain response, they did not provide explicit formulation of the plastic-strain-dependent elastic modulus degradation. Recently, Yoshida and Amaishi [31] proposed another type of nonlinear elastic model that is directly associated with the plastic-strain-dependent chord modulus model. In this model, the parameters in Eq.(1), E_o, E_a and ξ, were used for modeling with no additional material parameters being required. Based on this nonlinear elastic model, the yield-surface average (YSA) linear elastic model was also proposed as an extension of the chord modulus model.

To evaluate these linear and nonlinear elastic models in springback prediction, we (Yoshida and Amaishi [31]) conducted springback simulation using the Yoshida–Uemori [2–4] (Y-U) kinematic hardening (KH) model and found that the springback calculation results were close to those of previous (plastic-strain-dependent) linear elastic models, that is, the stress–strain nonlinearity played a minor role for springback prediction. However, other researchers [14, 26, 27] have reported that the consideration of nonlinear unloading stress–strain response significantly improves springback prediction. This is a completely different conclusion from our study. This situation suggests that springback prediction is affected not only by the elastic model, but also by the plasticity constitutive model used for the calculation.

To clarify what is necessary in elastic–plastic modeling for accurate springback simulation, in this study, two different types of plasticity models, the Y-U model as a pure KH model and the Armstrong–Frederick (A-F) KH [32] + isotropic hardening (IH) model as a combined KH + IH model, in combination with four linear/nonlinear elastic models, that is, a total of eight elastic–plastic models were examined. First, the accuracies of these models in describing the elastic–plastic transition behavior were discussed by comparing the stress-strain simulations with the corresponding experimental observations on DP980 AHSS and 590R HSS sheets. Then, by simulating the plane-strain uniform bending–unbending, the effect of the elastic–plastic models on the springback prediction was investigated, with a discussion of both the springback deformation and the residual stress.

Some hot-rolled HSS sheets exhibit an apparent yield plateau (YP) in the uniaxial stress–strain curve. However, to the best of our knowledge, the effect of YP on springback has never been investigated before, because it is usually neglected in springback simulation. In the present study, to determine whether the YP model is essential for an accurate springback prediction, the springback of 590R calculated by the YP model was compared with that obtained with the non-YP model.

Elasto-plasticity models

Framework of modeling

The strain rate, $\dot{\boldsymbol{\varepsilon}}$, is decomposed into its elastic and plastic parts, $\dot{\boldsymbol{\varepsilon}}^e$and $\dot{\boldsymbol{\varepsilon}}^p$, as follows:

$$\dot{\boldsymbol{\varepsilon}} = \dot{\boldsymbol{\varepsilon}}^e + \dot{\boldsymbol{\varepsilon}}^p. \quad (2)$$

The constitutive equation for elasticity is expressed by the equation:

$$\overset{o}{\boldsymbol{\sigma}} = \boldsymbol{C}^e : \dot{\boldsymbol{\varepsilon}}^e, \tag{3}$$

where $\overset{o}{\boldsymbol{\sigma}}$ denotes the objective rate of the Cauchy stress $\boldsymbol{\sigma}$ and $\boldsymbol{C}^e$is the elastic modulus tensor.

Using the yield function ϕ, the initial yielding is expressed using the following equation:

$$f = \phi(\boldsymbol{\sigma}) - Y_0 = 0, \tag{4}$$

where Y_0 denotes the initial yield strength. The subsequent yield condition after plastic deformation is generally given by the following equation, assuming the combined KH and IH of the yield surface:

$$\begin{aligned} f = \phi(\boldsymbol{\sigma} - \boldsymbol{\alpha}) - Y = \phi(\boldsymbol{\sigma} - \boldsymbol{\alpha}) - \left(Y_0 + R_{IH}\right) = 0, \\ Y = Y_0 + R_{IH}, \end{aligned} \tag{5}$$

where $\boldsymbol{\alpha}$ and Y are the position of the center and size of the subsequent yield surface, that is, the backstress and effective stress, respectively, and R_{IH} is the IH stress. The effective plastic strain p and its rate $\dot{p}$ are defined based on the plastic work conjugate concept, as follows:

$$Y\dot{p} = (\boldsymbol{\sigma} - \boldsymbol{\alpha}) : \dot{\boldsymbol{\varepsilon}}^p, \quad p = \int \dot{p}dt. \tag{6}$$

The associated flow rule is given by the following equation:

$$\dot{\boldsymbol{\varepsilon}}^p = \frac{\partial \phi}{\partial \boldsymbol{\sigma}}\dot{\lambda}, \tag{7}$$

where $\dot{\lambda}$ is the plastic multiplier, and $\dot{\lambda} = \dot{p}$, assuming the homogeneous yield function ϕ. Thus, the constitutive equation is expressed as follows:

$$\overset{o}{\boldsymbol{\sigma}} = \boldsymbol{C}^{ep} : \dot{\boldsymbol{\varepsilon}}, \tag{8}$$

$$\boldsymbol{C}^{ep} = \begin{cases} \boldsymbol{C}^e & \text{if } \dot{\lambda} = 0 \\ \boldsymbol{C}^e - \frac{\boldsymbol{C}^e : \frac{\partial \phi}{\partial \boldsymbol{\sigma}} \otimes \boldsymbol{C}^e : \frac{\partial \phi}{\partial \boldsymbol{\sigma}}}{\frac{\partial \phi}{\partial \boldsymbol{\sigma}} : \boldsymbol{C}^e : \frac{\partial \phi}{\partial \boldsymbol{\sigma}} + H} & \text{if } \dot{\lambda} > 0 \end{cases} \tag{9}$$

Here, H is the rate of workhadening which consists of the KH and IH components, H_{kin} and H_{iso}, as follows:

$$H = H_{kin} + H_{iso} \tag{10}$$

In this framework, each elasto–plasticity model is characterized by its elastic modulus $\boldsymbol{C}^e$, and the KH and IH laws of plasticity (i.e., the evolution equations of the backstress $\boldsymbol{\alpha}$ and IH stress R_{IH}).

Plastic-strain-dependent elastic models

Chord modulus model

As mentioned in the introduction, the chord modulus is measured using a sequential tensile loading–unloading experiment (Fig. 1c), and the three material parameters, E_o, E_a and ξ in Eq. (1) are determined. Note that in this experiment, the stress range σ_0 for measuring the elastic modulus is not a fixed value, but it increases with increasing plastic strain p because of the workhardening of the material. Therefore, the chord modulus is consistent with the modulus of the KH + IH model only for the case in which the yield surface expands following the condition $Y = Y_0 + R_{IH}(p) = \sigma_0(p)/2$. However, in practice, Eq. (1) is usually used for any elasto-plasticity model that follows the condition $Y \neq \sigma_0(p)/2$, including the case of the pure KH model ($R_{IH} = 0$).

Nonlinear elastic model

Figure 2 shows a schematic illustration of the nonlinear stress–strain unloading-reloading curve. The instantaneous elastic modulus, $E = d\sigma/d\varepsilon$ (hereafter it is called "elastic modulus"), varies from E_o(Young's modulus) at the unloading-start point a ($\sigma = \sigma_0$) to E_* at the fully unloaded point c ($\sigma = 0$). Note that.

$$E_{chord} \approx \frac{E_0 + E_*}{2}. \tag{11}$$

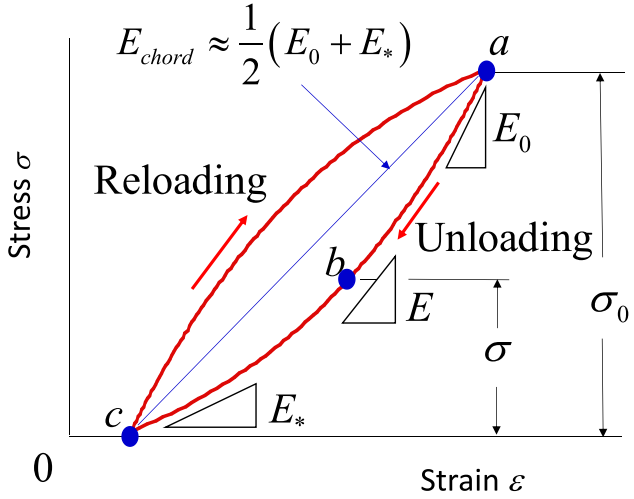

Fig. 2 Schematic illustration of the unloading–reloading stress–strain response

Assuming that the elastic modulus E varies as a linear function of the stress σ; using Eq. (11), the unloading elastic modulus is given by.

$$\begin{aligned} E &= E_* + \left(E_0 - E_*\right)\left(\frac{\sigma}{\sigma_0}\right) \\ &\approx E_0 - 2\left(E_0 - E_a\right)\left[1 - \exp\left(-\xi p\right)\right]\left(\frac{\sigma_0 - \sigma}{\sigma_0}\right). \end{aligned} \tag{12}$$

Using Eq. (12), the elastic modulus at a stress point existing inside the yield surface of its size Y (see schematic illustrations in Fig. 3) is expressed as follows:

$$E = E_0 - 2\left(E_0 - E_a\right)\left[1 - \exp\left(-\xi p\right)\right]\left(\frac{2Y - \rho}{\sigma_0}\right), \tag{13}$$

where ρ is the distance from the current stress point b ($\sigma = \sigma$) to a point d lying on the yield surface when the direction of the stress increment $d\sigma$ is $b \to c$. Note that when $\rho = 0$ at point d,

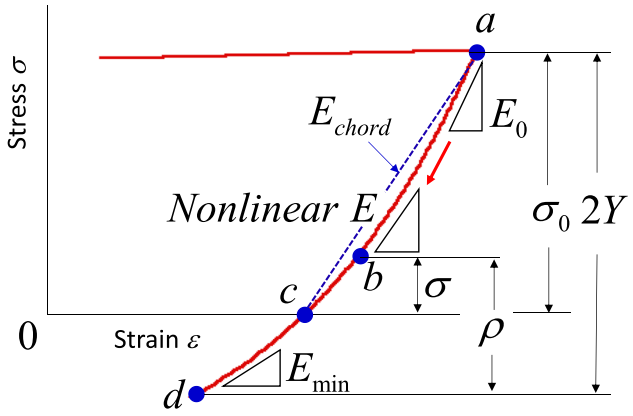

Fig. 3 Stress-state-determined nonlinear elastic modulus

$$E = E_{\min} = E_0 - 2\left(E_0 - E_a\right)\left[1 - \exp\left(-\xi p\right)\right]\left(\frac{2Y}{\sigma_0}\right). \tag{14}$$

The nonlinear elastic model in Eq. (13) is also valid for the multiaxial stress state, where ρ is defined as schematically illustrated in Fig. 4a. In the yield surface, a linear elastic response domain (surface) f_{LER} of size κ ($<Y$) and center $\boldsymbol{\eta}$ is assumed (hereafter f_{LER} called "LER surface"):

$$f_{LER} = \phi(\boldsymbol{\sigma} - \boldsymbol{\eta}) - \kappa \le 0. \tag{15}$$

The stress point $\boldsymbol{\sigma}$ exists either inside or on the LER surface. If the stress point moves inside of the LER surface, the stress–strain response is linear,

$$\overset{o}{\boldsymbol{\sigma}} = \boldsymbol{C}_L^e : \dot{\boldsymbol{\varepsilon}} \text{ if } f_{LER} < 0, \text{or } f_{LER} = 0 \text{ and } \frac{\partial f_{LER}}{\partial \boldsymbol{\sigma}} : \overset{o}{\boldsymbol{\sigma}} < 0, \tag{16}$$

where $\boldsymbol{C}_L^e$ is the fixed-value elastic stiffness matrix composed of the elastic modulus E_{LER} (see Fig. 4b) and Poisson's ratio. If the stress point lies on the LER surface and moves outward, the constitutive equation is given by the following equation,

$$\overset{o}{\boldsymbol{\sigma}} = \boldsymbol{C}_{NL}^e : \dot{\boldsymbol{\varepsilon}} \text{ if } f_{LER} = 0 \text{ and } \frac{\partial f_{LER}}{\partial \boldsymbol{\sigma}} : \overset{o}{\boldsymbol{\sigma}} \ge 0, \tag{17}$$

where $\boldsymbol{C}_{NL}^e$ is the stress-state-dependent elastic modulus tensor and is defined as follows:

$$\boldsymbol{C}_{NL}^e = \left(\frac{E}{E_0}\right)\boldsymbol{C}_0^e. \tag{18}$$

The definition of ρ under the multiaxial stress state is given by the following equation (Fig. 4a):

$$\begin{aligned} \rho &= \left\|\boldsymbol{\sigma}_* - \boldsymbol{\sigma}\right\| = \phi\left(\boldsymbol{\sigma}_* - \boldsymbol{\sigma}\right), \\ \boldsymbol{\sigma}_* &= \left(\frac{Y}{\kappa}\right)(\boldsymbol{\sigma} - \boldsymbol{\eta}) + \boldsymbol{\alpha}. \end{aligned} \tag{19}$$

The evolution equation of the LER-surface center, $\boldsymbol{\eta}$, is explicitly determined from the consistency condition (for details, refer to Yoshida et al. [33]):

$$\overset{o}{\boldsymbol{\eta}} = \frac{\frac{\partial f_{LER}}{\partial \boldsymbol{\sigma}} : \overset{o}{\boldsymbol{\sigma}}}{\frac{\partial f_{LER}}{\partial \boldsymbol{\sigma}} : \left(\boldsymbol{\sigma}_* - \boldsymbol{\eta}\right)} : \left(\boldsymbol{\sigma}_* - \boldsymbol{\eta}\right). \tag{20}$$

The yield-surface average (YSA) elastic modulus model

The chord modulus defined in the range of the yield surface is called the YSA elastic modulus (Fig. 5), and is easily derived from Eq. (14), as follows:

$$\begin{aligned} E_{YSA} &= \tfrac{1}{2}\left(E_0 + E_{\min}\right) \\ &= E_0 - \left(E_0 - E_a\right)\left[1 - \exp\left(-\xi p\right)\right]\left(\frac{2Y}{\sigma_0}\right). \end{aligned} \tag{21}$$

Cyclic plasticity models

Y-U model

The Y-U model is a pure KH model, wherein the yield surface of size Y_0 and center $\boldsymbol{\alpha}$ kinematically moves within the bounding surface, as illustrated in Fig. 6a. The bounding surface, F, isotropically expands from its initial size B to

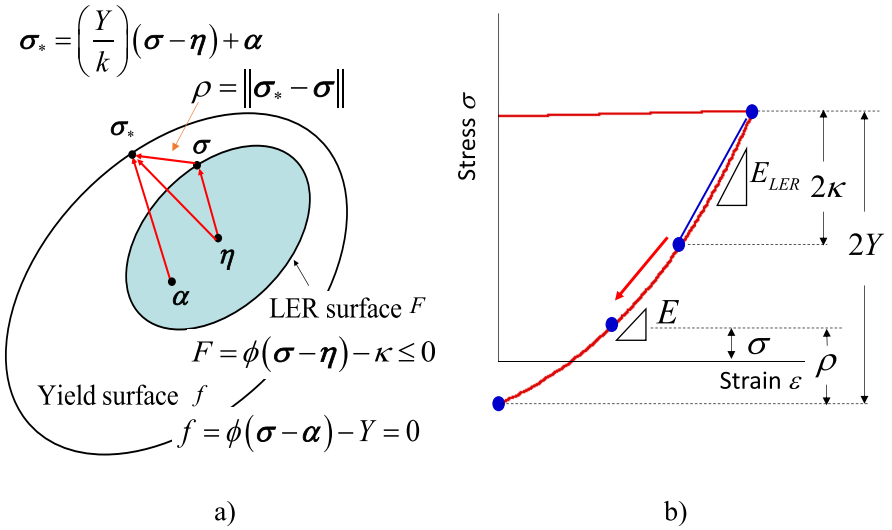

Fig. 4 Determination of the nonlinear elastic modulus under multiaxial stress state. a) LER surface moving in the yield surface, b) Uniaxial stress–strain response

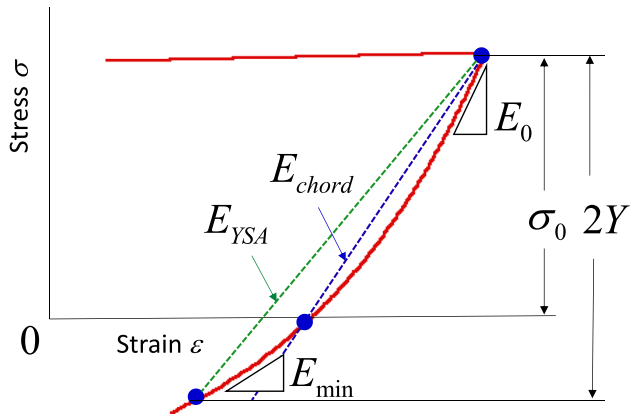

Fig. 5 YSA elastic modulus

$B+R$, and its center $\boldsymbol{\beta}$ moves kinematically with increasing plastic strain. The relative motion of the yield surface with respect to the bounding surface.

$$\boldsymbol{\alpha}_* = \boldsymbol{\alpha} - \boldsymbol{\beta} \tag{22}$$

is given by the following evolution equation:

$$\overset{o}{\boldsymbol{\alpha}}_* = C\left\{\left(\frac{a}{Y_0}\right)(\boldsymbol{\sigma}-\boldsymbol{\alpha}) - \sqrt{\frac{a}{\bar{\alpha}_*}}\boldsymbol{\alpha}_*\right\}\dot{p}, \tag{23}$$

$$\bar{\alpha}_* = \phi(\Longleftarrow_*), a = B + R - Y_0. \tag{24}$$

Here, a material parameter C takes one of two values, $C = C_1$ for a region in the vicinity of the initial yielding,

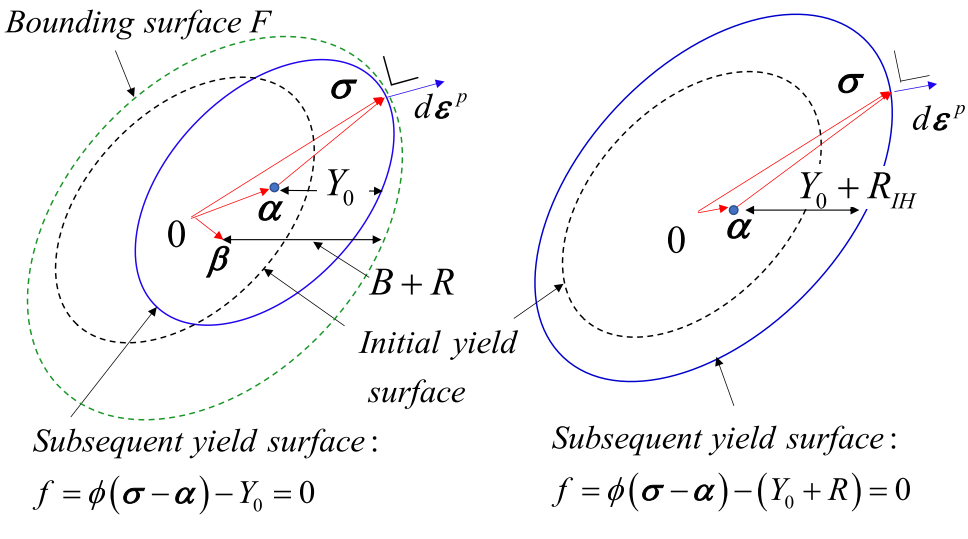

Fig. 6 -U pure KH model and A-F KH + IH model

Table 1 Y-U parameters for DP980 AHSS

(a) Plasticity parameters							
Y_0(MPa)	B(MPa)	b(MPa)	R_{sat}(MPa)	C_1	C_2	k	h
500	970	90	90	300	160	20.0	0.35
(b) Plastic-strain–dependent chord modulus of elasticity							
E_0(GPa)	E_a(GPa)	ξ					
206	160	90					

Table 2 Y-U parameters for 590R HSS

(a) Plasticity parameters							
Y_0(MPa)	B(MPa)	b(MPa)	R_{sat}(MPa)	C_1	C_2	k	h
320	450	100	210	250	220	16.0	0.8
(b) Plastic-strain-dependent chord modulus of elasticity							
E_0(GPa)	E_a(GPa)	ξ					
208	160	80					

*when considering the yield plateau (YP), Y_p = 420MPa.

and $C = C_2$ for the other plastic deformation processes. The kinematic motion of $\boldsymbol{\beta}$ is given by the following equation:

$$\overset{o}{\boldsymbol{\beta}} = k\left\{\left(\frac{b}{Y_0}\right)(\boldsymbol{\sigma}-\boldsymbol{\alpha})-\boldsymbol{\beta}\right\}\dot{p}, \tag{25}$$

where b and k are material parameters. For the isotropic hardening of the bounding surface, the evolution of R is given by the following equation based on the Voce hardening law:

$$\dot{R} = k\left(R_{sat}-R\right)\dot{p}, \tag{26}$$

where k and R_{sat} are material parameters. In addition to the Voce-type IH model, the use of a combination of the Voce and Swift hardening law for the evolution of R is also available (refer to Yoshida et al., 2015 [33]). One of the features of the Y–U model is that it describes the *workhardening stagnation* that appears in a reverse stress–strain curve for a certain range of reverse deformation. To control its strength, a material parameter h is used in the Y-U model (a larger h-value predicts more workhardening stagnation, for details, refer to Yoshida et al. [3, 4]). The rate of workhardening H in the Y-U model is expressed as follows:

$$H = H_{kin} = Ca + kb - \frac{\partial\phi}{\partial\boldsymbol{\sigma}} : \left(C\sqrt{\frac{a}{\overline{\alpha}_*}}\boldsymbol{\alpha}_* + k\boldsymbol{\beta}\right). \tag{27}$$

A-F KH + IH model

In the combined KH + IH model, the yield surface moves kinematically with expansion, as illustrated in Fig. 6b. The A-F KH law is given by the following equation:

Table 3 A-F + IH parameters for DP980 AHSS

(a) Plasticity parameters				
Y_0(MPa)	a_{A-F}(MPa)	Q(MPa)	C_{A-F}	m
700	300	120	70	12.0
(b) Plastic-strain-dependent chord modulus of elasticity				
E_0(GPa)	E_a(GPa)	ξ		
206	160	90		

$$\overset{o}{\boldsymbol{\alpha}} = C_{A-F}\left\{\left(\frac{a_{A-F}}{Y_0+R_{IH}}\right)(\boldsymbol{\sigma}-\boldsymbol{\alpha})-\boldsymbol{\alpha}\right\}\dot{p}, \tag{28}$$

where C_{A-F} and a_{A-F} are material constants. For the isotropic hardening law, the following Voce type equation is assumed:

$$\dot{R}_{IH} = m\left(Q-R_{IH}\right)\dot{p}, \tag{29}$$

where m and Q are material parameters. The rate of workhardening, H, in this model is expressed as follows:

$$H = H_{kin} + H_{iso} = C_{A-F}a_{A-F} - C_{A-F}\frac{\partial\phi}{\partial\boldsymbol{\sigma}} : \boldsymbol{\alpha} + m\left(Q-R_{IH}\right). \tag{30}$$

The stress–strain responses of the DP980 and 590R sheets that were calculated using the Y-U model (material parameters are listed in Tables 1 and 2) and the A-F + IH model (for material parameters, see Tables 3 and 4) are illustrated in Figs. 7 and 8, respectively. For both models, the chord modulus of elasticity was used. For DP980, both models are able to describe the workhardening and the Bauschinger effect fairly well. However, in the A-F + IH model simulation, an apparent corner at the re-yielding point in the unloading stress–strain curve was found, but

Table 4 A-F + IH parameters for 590R HSS

(a) Plasticity parameters				
Y_0(MPa)	a_{A-F}(MPa)	Q(MPa)	C_{A-F}	m
320	180	270	100	10.0
(b) Plastic-strain-dependent chord modulus of elasticity				
E_0(GPa)	E_a(GPa)	ξ		
208	160	80		

*when considering YP, $Y_p = 420$MPa

it was not so clearly observed in the Y-U model simulation (see the next section for a more detailed discussion). Furthermore, for the 590R, the A-F + IH model overestimated the cyclic workhardening, whereas the Y-U model well simulate the uniaxial tension and cyclic stress-strain responses. This is because only one A-F KH variable is insufficient in describing cyclic behavior properly, and furthermore modeling of the workhardening stagnation is lacking in the A-F + IH model (successful description of cyclic workhardening of the 590R was only possible when using a strong workhardening-stagnation parameter $h =$

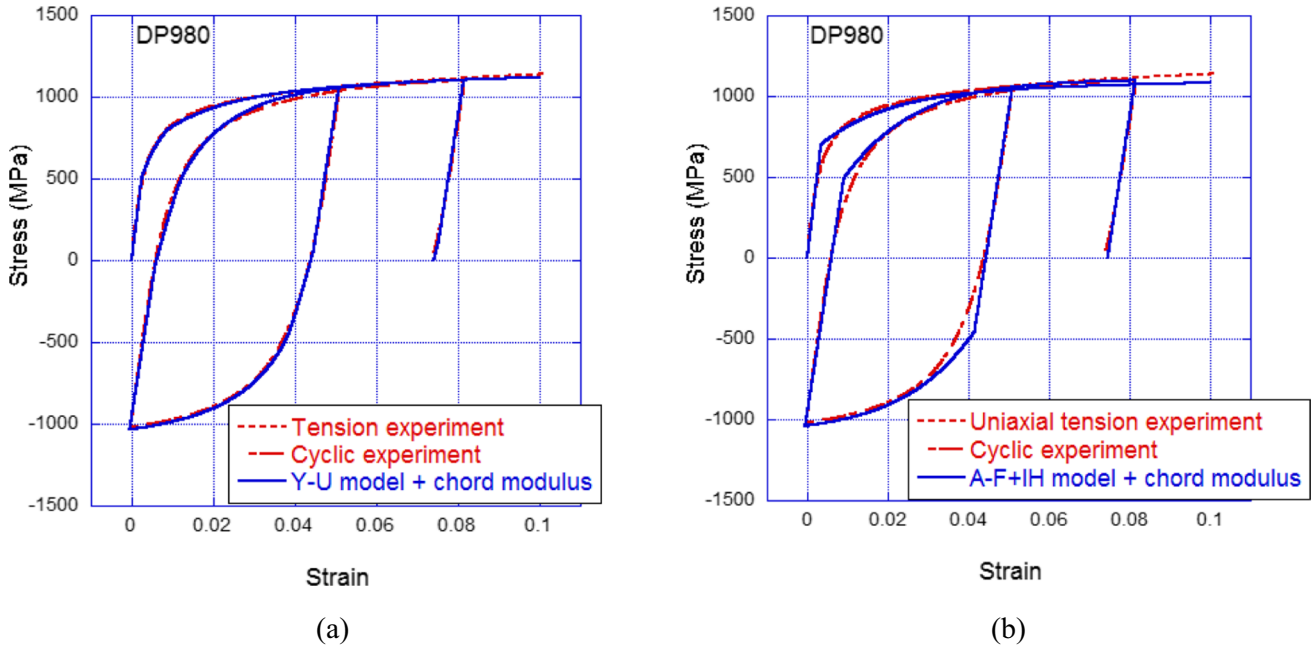

Fig. 7 Uniaxial tension and cyclic stress-strain responses on the DP980 calculated by (**a**) Y-U model, and (**b**) A-F + IH model, where the chord modulus of elasticity is used for both models

Fig. 8 Uniaxial tension and cyclic stress–strain responses on the 590R calculated by (**a**) Y-U model, and (**b**) A-F + IH model, where the chord modulus of elasticity is used for both models

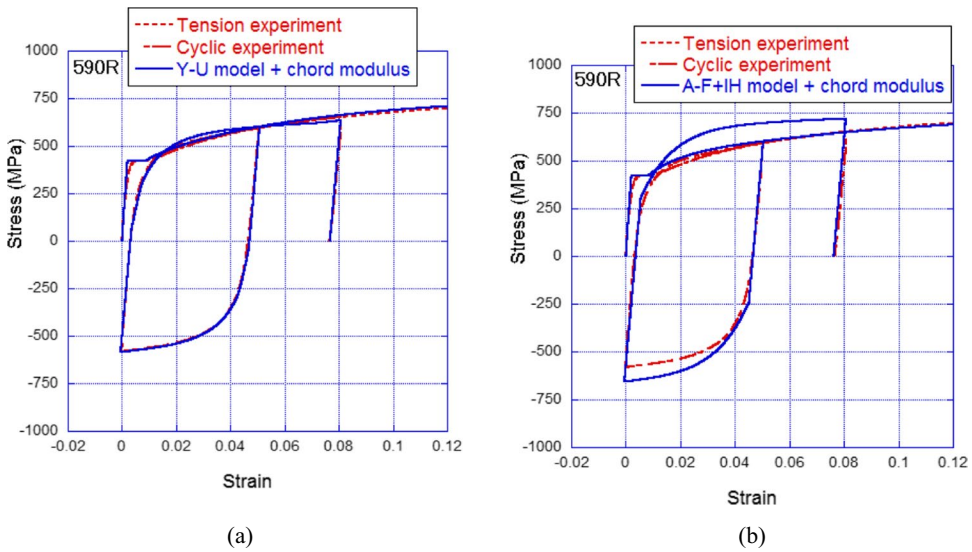

0.8 in the Y-U model). However, instead of using one A-F KH variable (Eq. (28)), if the backstress $\boldsymbol{\alpha}$ is composed of several A-F KH components, $\boldsymbol{\alpha} = \sum_{i=1}^{M} \boldsymbol{\alpha}_i^{A-F}$, proposed by Chaboche et al. [34, 35], the description of elastic-plastic transition and cyclic hardening behaviors will be improved. However, it has a drawback in that an increase in the number of KH components leads to a significant increase in the computational cost.

Description of elastic–plastic transition behaviors in reverse deformation

The amount of springback is determined as a function of the bending moment at the final stage of the forming and the unloading stress–strain behavior. In this section, the significance of the description of the unloading elastic–plastic transition behavior is discussed based on the DP980 simulation data. The 590R was used to examine the effect of YP on springback.

The DP980 stress–strain curves during unloading and the subsequent compression calculated by the Y-U model are illustrated in Figs. 9a and b, using several linear elastic models (Fig. 9a) and nonlinear elastic model (Fig. 9b). From these figures, it was found that the stress–strain responses calculated by the chord modulus and YSA elasticity modulus models are almost the same, and are not very far from those calculated by the nonlinear elastic model. The results of calculated by these models, except for the Young's modulus case, agree fairly well with the experimental observations. For example, the flow stress of the DP980 at 0.05 strain (0.045 plastic strain), $\sigma_0 = 1060$ MPa, is almost the same as the value of $2Y_0 = 1000$ MPa. Also, the values of the chord modulus, 160 GPa, and the YSA modulus, 161 GPa, become almost the same. The elastic–plastic stress–strain slope at the re-yielding point is:

$$d\sigma/d\varepsilon|_{re-yield}^{\text{Y-U}} = \frac{E_0 H_{kin}}{E_0 + H_{kin}} \approx 85 \text{ GPa, where } H_{kin} \approx 2Ca = 145 \text{ GPa.} \tag{31}$$

This is not very far from the nonlinear elastic modulus at the re-yielding point, $E_{\min} = 121$ GPa. Therefore, the Y-U model combined with the nonlinear elastic modulus can be used to successfully describe the smooth elastic-plastic stress–strain transition behavior. Even when using $E_{chord} = 160$ GPa or $E_{YSA} = 161$ GPa, the calculated elastic-plastic stress–strain transition behavior is acceptable.

In contrast to the Y-U model, the stress–strain curves calculated by the A-F + IH model are different depending on the elastic models used in the calculation. When using the linear elastic models, as shown in Fig. 10a, clear corners of the stress–strain curves appear at the re-yielding points, while a comparatively smoother unloading stress–strain response is simulated by the nonlinear elastic model (see Fig. 10b). Such a difference in the elastic-plastic transition behavior between the Y-U model and the A-F + IH model is mostly due to the difference in the backstress recall terms (compare Eq. (23) to (28)). Furthermore, the size of yield surface of the Y-U model is fixed constant, but that of the A-F + IH model expands with increasing plastic strain; it affects the elastic-plastic transition description. For the 0.045 plastic pre-strain, the nonlinear elastic modulus at the re-yielding point is $E_{\min}^{\text{A-F+IH}} = 70$ GPa, while $E_{chord} = 160$ GPa and $E_{YSA} = 137$ GPa. The diameter of the yield surface in the A-F + IH model, $2Y = 2(Y_0 + R_{IH}) = 1540$ MPa, is much larger than the uniaxial tension flow stress $\sigma_0 = 1060$ MPa, which is why the YSA elastic modulus becomes smaller than the chord modulus (Eqs. (1) and (21)). Note that the nonlinear elastic modulus of the AF + IH model at the re-yielding point, $E_{\min}^{\text{A-F+IH}} = 70$ GPa when $p = 0.045$, is much smaller than that of the Y-U model, $E_{\min}^{\text{Y-U}} = 121$ GPa, because the yield strength of the AF +

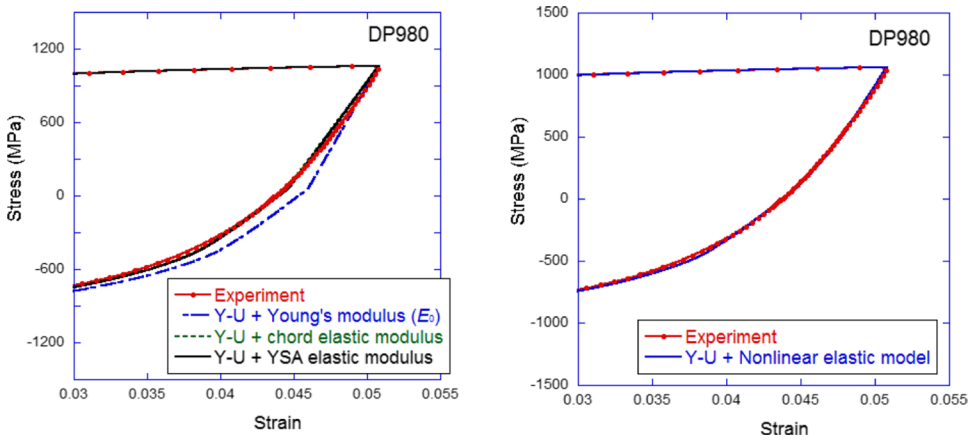

a) Linear elastic models b) Nonlinear elastic models

Fig. 9 Elastic–plastic transition behaviors calculated from the Y-U model combined with several types of linear elasticity models

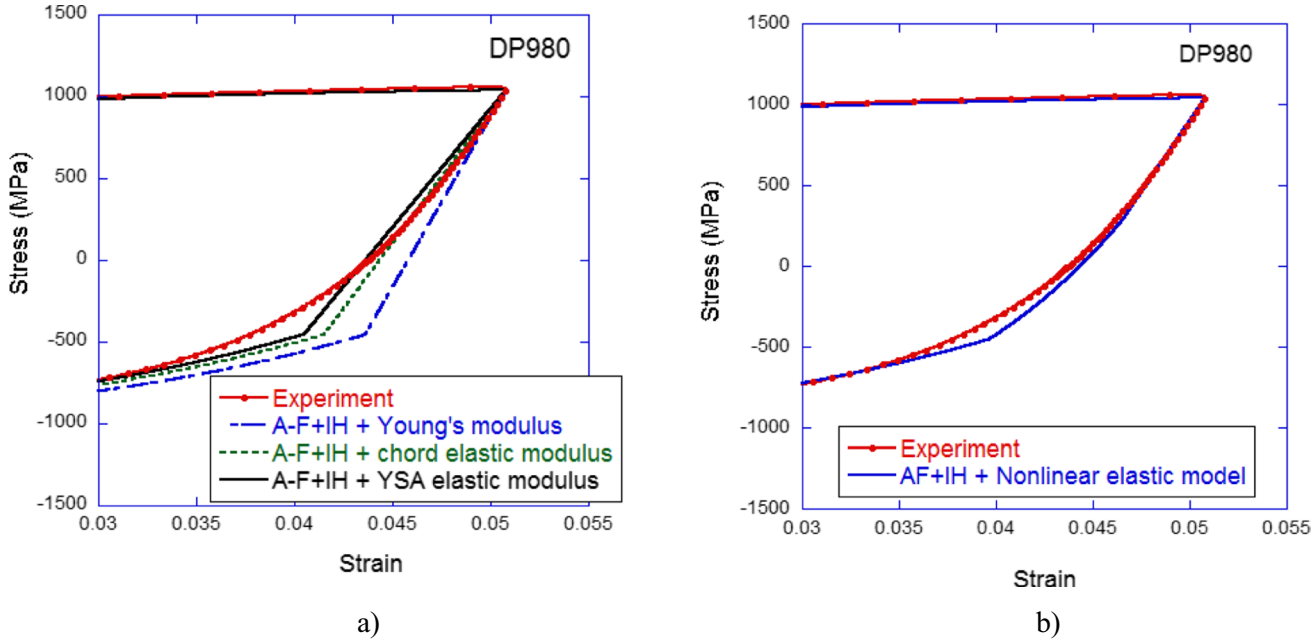

Fig. 10 Elastic–plastic transition behaviors calculated by the A-F + IH model combined with several types of linear elasticity models. **a** Linear elastic models, **b** Nonlinear elastic models

IH model, $Y = Y_0 + R_{IH} = 770$ MPa, is larger than that of the Y-U pure KH model, $Y = Y_0 = 500$ MPa. The workhardening rate of the AF + IH model at the re-yielding point is.

$$\begin{aligned} H_{kin} &\approx 2C_{A-H}a_{A-H} = 42 \text{ GPa}, \\ H_{iso} &= m\left(Q - R_{IH}\right) = mQ\exp\left(-mp\right) \approx 1 \text{ GPa}, \\ H &= H_{iso} + H_{kin} \approx 43 \text{ GPa}, \end{aligned} \tag{32}$$

then the elastic–plastic stress-strain slope there is calculated as:

$$d\sigma/d\varepsilon|_{re-yield}^{\text{A-F+IH}} = \frac{E_0 H}{E_0 + H} \approx 36 \text{ GPa}. \tag{33}$$

Although this value of 36 GPa is considerably smaller than 85 GPa obtained in the Y-U model, (Eq. (31)), the elastic modulus at the elastic limit (re-yielding point) is also as low as $E_{\min}^{\text{A-F+IH}} = 70$ GPa; therefore the description of the smooth elastic-plastic transition becomes possible in the AF + IH calculation by using the nonlinear elastic model.

Effect of material models on springback prediction

Analytical model of springback

Springback simulations for the two forming-springback processes, that is, the uniform bending and the bending–unbending under the plane-strain condition, were conducted to investigate the effect of description of the elastic–plastic transition behavior on the springback prediction. An advantage of using such a simple analytical model is that the numerically obtained results of springback are totally free from experimental noise such as die/sheet friction and die deflection; therefore, it is suitable for the discussion of material-model-dependent springback prediction.

The bending–unbending springback scheme is as follows: Let the x-, y-, and z-coordinates be the longitudinal, width and thickness directions of a sheet,respectively, as illustrated in Fig. 11. Neglecting the variation in sheet thickness, the bending strain rate $\dot{\varepsilon}_x$ is expressed by the following equation based on the Kirchhoff–Love hypothesis:

$$\dot{\varepsilon}_x = \dot{\kappa} z, \tag{34}$$

where $\dot{\kappa}$ is the rate of the curvature of the sheet. For the analysis of the bending and unbending processes, the following 2D ($\dot{\sigma}_z = 0$) constitutive model of elasto-plasticity was used:

$$\begin{Bmatrix} \dot{\sigma}_x \\ \dot{\sigma}_y \end{Bmatrix} = \begin{bmatrix} C_{11}^{ep} & C_{12}^{ep} \\ C_{21}^{ep} & C_{22}^{ep} \end{bmatrix} \begin{Bmatrix} \dot{\varepsilon}_x \\ \dot{\varepsilon}_y \end{Bmatrix}, \tag{35}$$

where, $\dot{\varepsilon}_y = 0$ for the plane-strain condition. In the calculation, the von Mises yield criterion was assumed because the purpose of this study was to clarify the effects of elasticity modeling and the Bauschinger effect, but not the effect of sheet anisotropy. Furthermore, the plane-strain stresses of DP980 and 590R were not very far from the von Mises

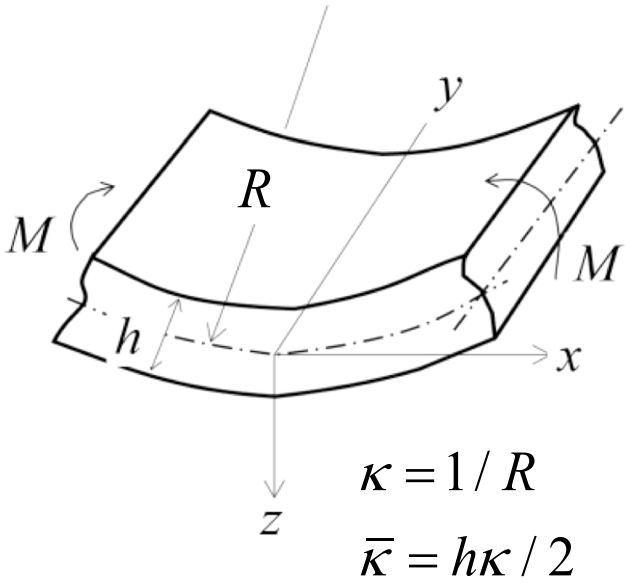

Fig. 11 Schematic illustration of plane-strain bending

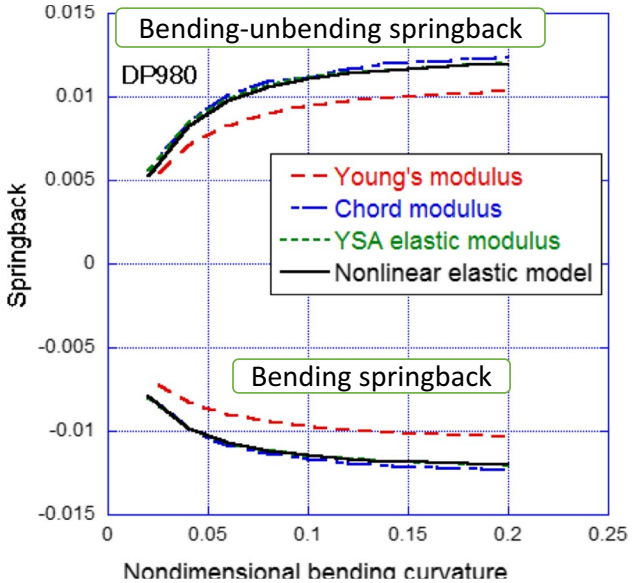

Fig. 12 Springback of the DP980 calculated by Y-U model with several types of elastic models

calculation (see Appendix). The rate of the bending moment $\dot{M}$ is calculated for a given rate of curvature $\dot{\kappa}$, as follows:

$$\dot{M} = \int \dot{\sigma}_x z dz = \dot{\kappa} \int C_{11}^{ep} z^2 dz \tag{36}$$

For the bending springback, the bending moment up to a given nondimensional curvature $\bar{\kappa} = h\kappa/2 = \bar{\kappa}_0$ (h: sheet thickness), $M = M_0$, was first calculated, and then the springback curvature $\Delta\bar{\kappa}$ was obtained from the process of $M \to 0$. For the bending-unbending springback, an unbending process $\bar{\kappa} = \bar{\kappa}_0 \to 0$ was added before the springback. The residual stresses were obtained at the final stage of springback. In the following discussion, the residual stresses at the outer surface of the sheet was used.

Discussion of springback and residual stresses

The springback $\Delta\bar{\kappa}$ of the DP980, as a function of the nondimensional bending curvature $\bar{\kappa}_0$, calculated using the Y-U model with several elastic models is illustrated in Fig. 12. For both bending and bending-unbending processes, the springback predictions for two plastic-strain dependent elastic models, the chord modulus and YSA elastic models, and the nonlinear elastic model are close to each other (the differences in springback calculated by the two linear elastic models from the nonlinear model calculation were less than 4%), whereas when using the Young's modulus, E_0 (= a fixed value, 206 GPa), it is underestimated because of the overestimation of the bending rigidity. Fig. 13 shows the bending moment vs. nondimensional curvature curves in the bending-unbending springback ($\bar{\kappa}_0 = 0.2$), where almost the same amounts of final springback were calculated by the chord modulus, YSA modulus and the nonlinear elastic

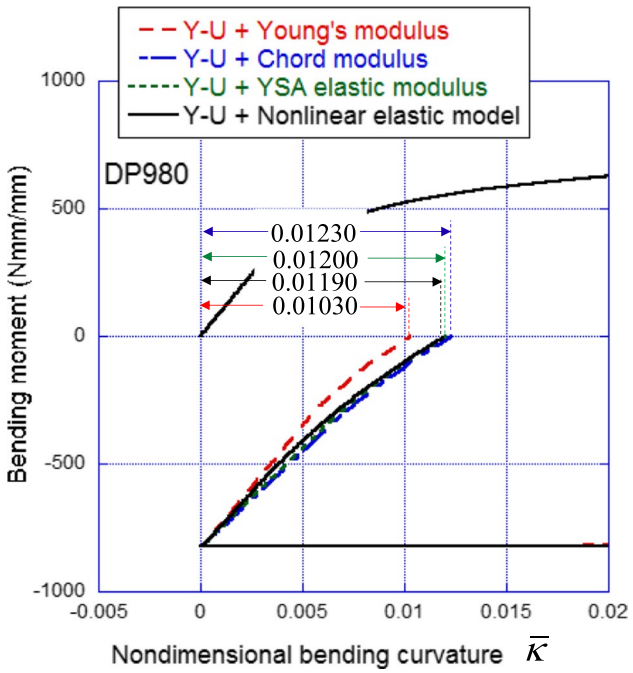

Fig. 13 Bending moment vs. nondimensional curvature curves for the bending–unbending springback ($\bar{\kappa}_0 = 0.2$)

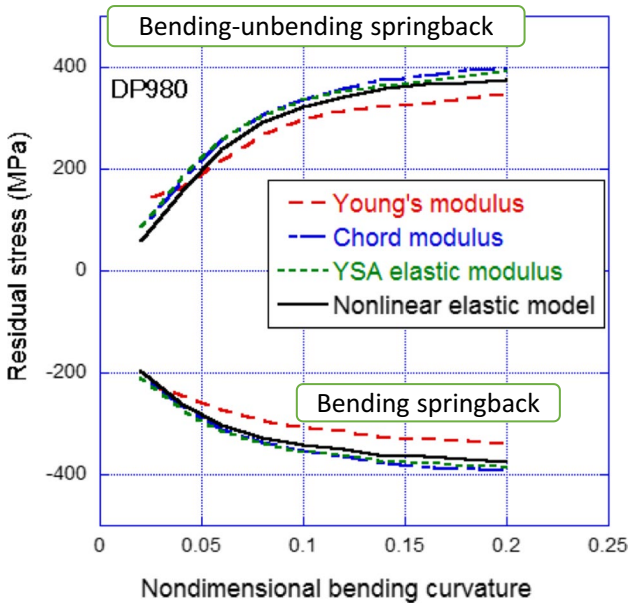

Fig. 14 Residual stresses in the DP980 calculated by Y-U model in combination with several types of elastic models

models, although the moment–curvature responses during springback are slightly different depending on these elastic models. As illustrated in Fig. 14, the residual stresses predicted by the Y-U model were approximately the same, irrespective of the type of elastic model. The calculation errors of the residual stresses calculated by the linear models were less than 6%, compared with the nonlinear model calculation. Fig. 15 shows the stress–strain response of the outer surface of the sheet for the bending-unbending springback ($\overline{\kappa}_0 = 0.2$), where re-yielding occurs during the springback at $\sigma_x \approx -206 \sim -222$ MPa for all the calculations. From the above results, it can be concluded that, when using the Y-U model, the calculations of springback and residual stress are not significantly affected by the types of elastic models if the plastic-strain–dependent elastic modulus degradation is properly modeled. This is because, in the Y-U model calculation, the elastic–plastic stress–strain transition calculated by these models is sufficiently smooth, even when using linear elastic models (Fig. 9a and b).

In contrast to the Y-U model, when using the A-F + IH model, the springback prediction differs depending on the elastic modulus models (the difference in springback between the chord modulus and the nonlinear model calculations reaches 7%), as illustrated in Figs. 16 and 17. This is because the description of the elastic–plastic transition behavior during the springback process strongly affects the final amount of springback (Figs. 10a and b). The residual stresses in the DP980 calculated by the A-F + IH model in combination with several elastic models are illustrated in Fig. 18. The stress-strain response during the springback after bending–unbending, for the case of $\overline{\kappa}_0 = 0.2$ is shown in Fig. 19. In all these calculations, re-yielding did not occur during springback, which is completely different from the Y-U model calculations where the springback was treated as an elastic–plastic deformation process (see Fig. 15). From Figs. 18 and 19, it was found that the level

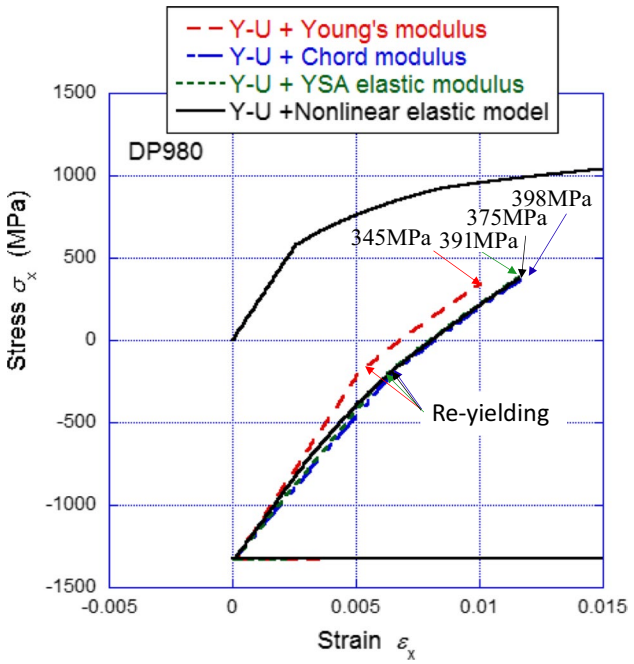

Fig. 15 Stress–strain responses in bending-unbending springback ($\overline{\kappa}_0 = 0.2$) of the DP980 calculated by the Y-U model in combination with several types of elastic models

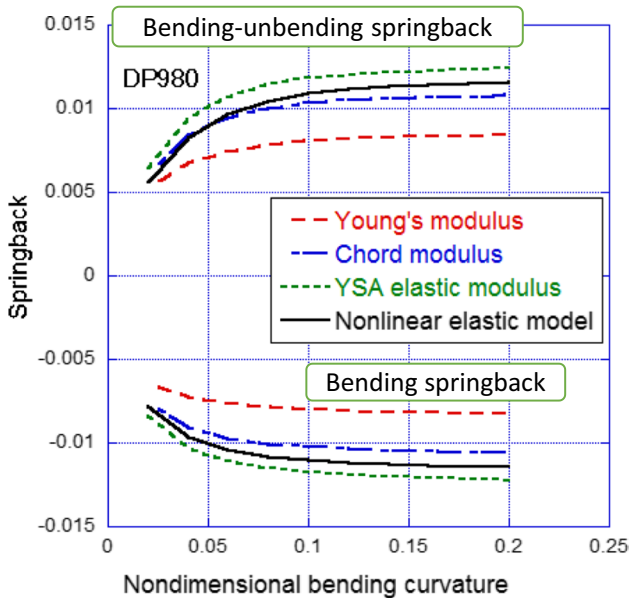

Fig. 16 Springback of DP980 calculated by A-F + IH model in combination with several types of elastic models

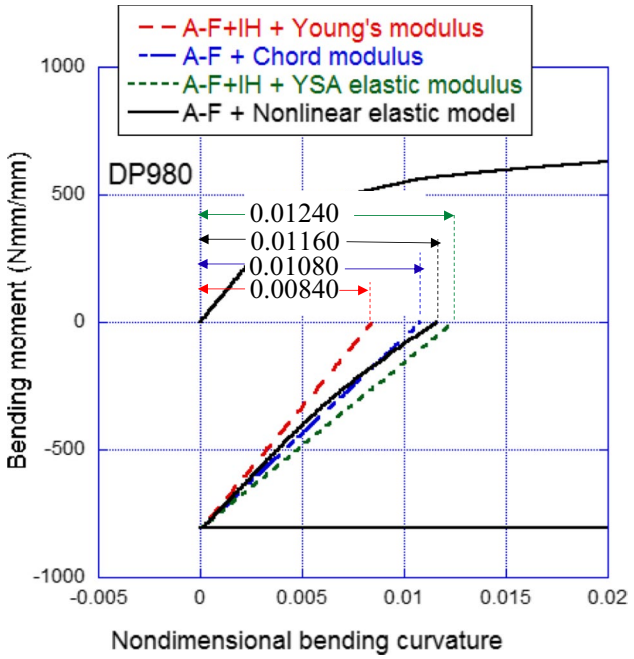

Fig. 17 Bending moment vs. nondimensional curvature curves in the bending–unbending springback ($\overline{\kappa}_0 = 0.2$)

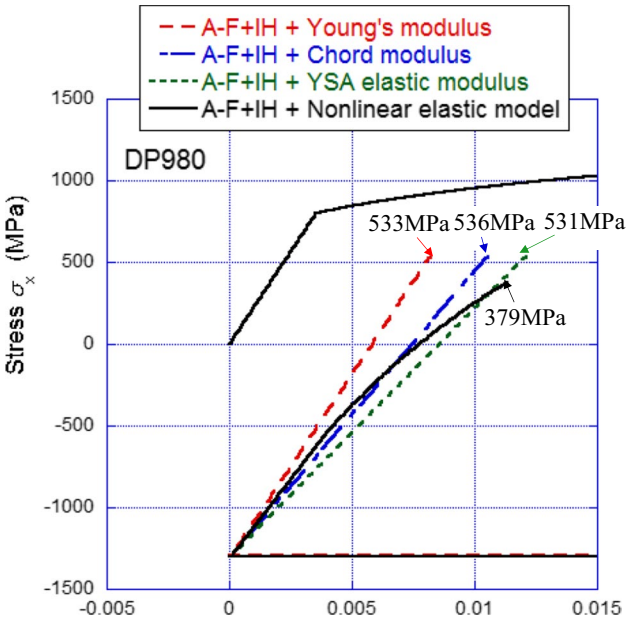

Fig. 19 Stress–strain responses in the bending-unbending springback ($\overline{\kappa}_0 = 0.2$) of the DP980, calculated by the A-F + IH model in combination with several types of elastic models

of residual stresses calculated by the linear elastic models is much higher than that of the nonlinear elastic model calculation (14% calculation error at a maximum). Interestingly, the springback and residual stress predicted by the A-F + IH model with the nonlinear elastic model are not very different from the results calculated by the Y-U model, as illustrated in Figs. 20 and 21. The use of the nonlinear elastic model is essential for A-F + IH springback analysis.

Effect of yield-plateau modeling on springback prediction

The 590R exhibited an apparent YP in the stress–strain curve, as illustrated in Fig. 22. It is a matter of interest to examine

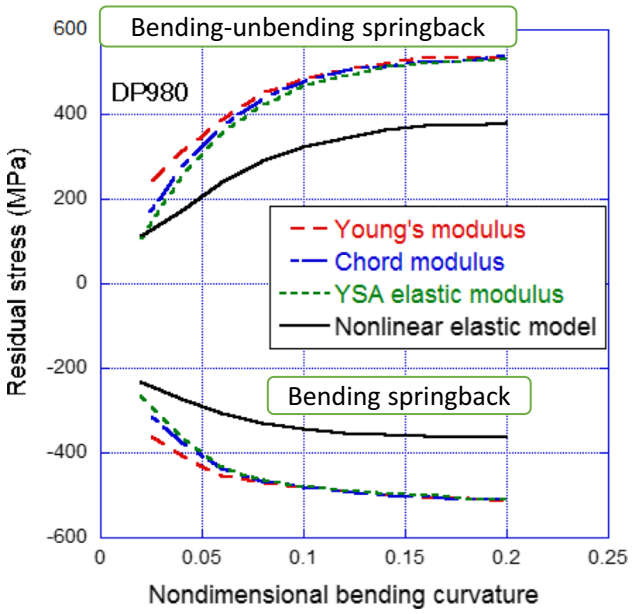

Fig. 18 Residual stresses in the DP980 calculated by A-F + IH model in combination with several types of elastic models

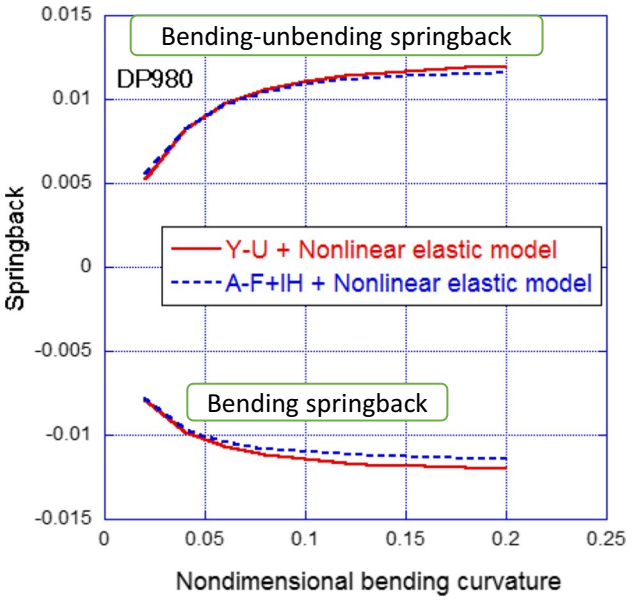

Fig. 20 Comparison of the springback calculated by Y-U and A-F + IH models when using nonlinear elastic model

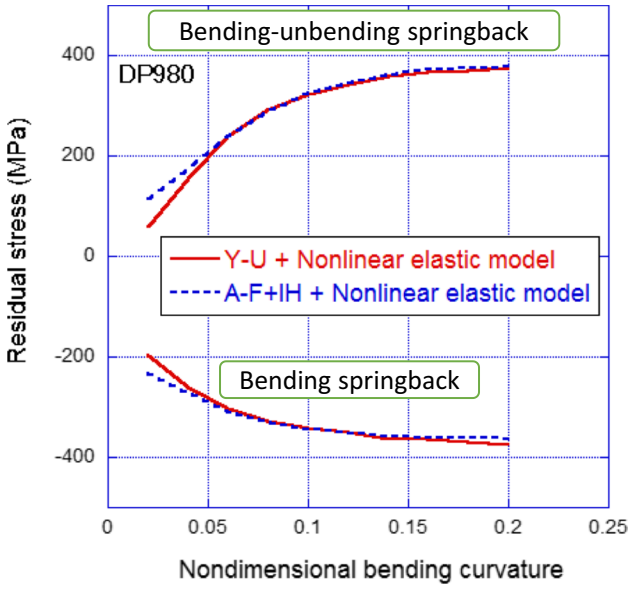

Fig. 21 Comparison of the residual stresses calculated by Y-U and A-F + IH models when using nonlinear elastic model

whether the YP stress–strain behavior strongly influences the springback, or it is a minor effect. To investigate this, two types of the Y-U model, one including the YP and the other excluding it (Fig. 22, denoted by "non-YP"), were employed for the springback simulation. For the modeling of the YP, the

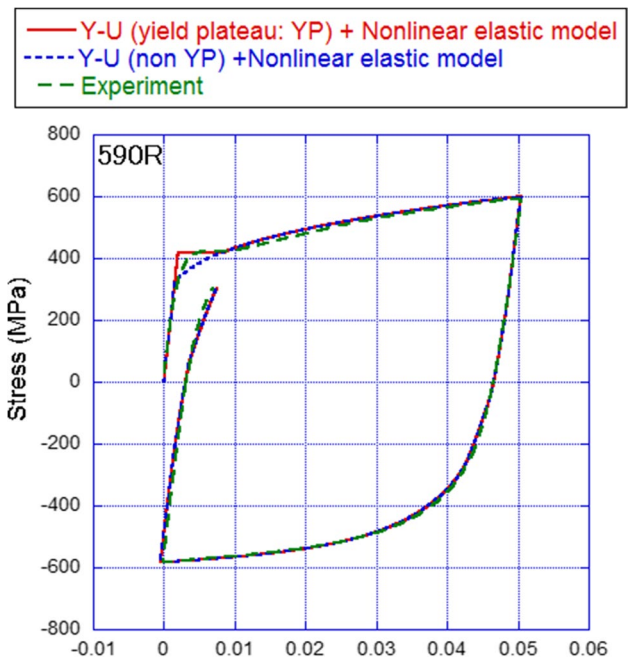

Fig. 22 Cyclic stress–strain responses on the 590R calculated by Y-U model with, without consideration of the yield plateau (YP)

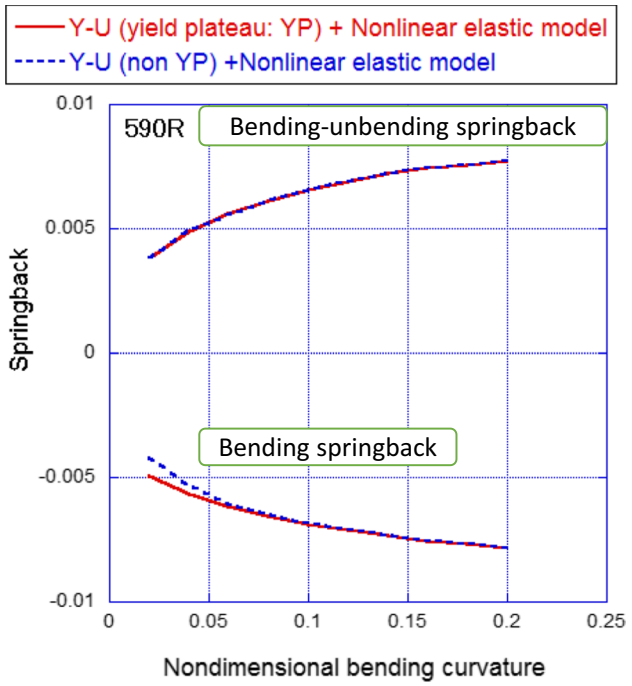

Fig. 23 Springback of 590R calculated by Y-U model with and without consideration of YP, while using the nonlinear elastic model

present authors (Yoshida [36], Yoshida et al. [37]) previously proposed a rate-dependent plasticity model that describes the sharp yield point and the subsequent abrupt yield drop as a consequence of the shear-stress–dependent dislocation motion and the rapid dislocation multiplication. However, in this discussion, a much simpler rate-independent Y-U model that assumes $H_{kin}=0$ at YP was employed. Figs. 23 and 24 show the springback and residual stresses on the 590R, respectively, calculated by the Y-U model with the nonlinear elastic model. From these figures, it was found that the effect of the YP on the calculations is limited only for the case of small-scale bending with $\overline{\kappa}_0 < 0.05$. Most calculations of the springback and residual stresses are unaffected by the type of plastic-strain–dependent elastic modulus models used in the Y-U model, as illustrated in Figs. 25 and 26. This is the same conclusion as one obtained for the DP980 case.

Summary and concluding remarks

This paper discusses the role of a material model for accurate springback simulation, specifically focusing on the effect of elastic–plastic transition behavior. Three types of

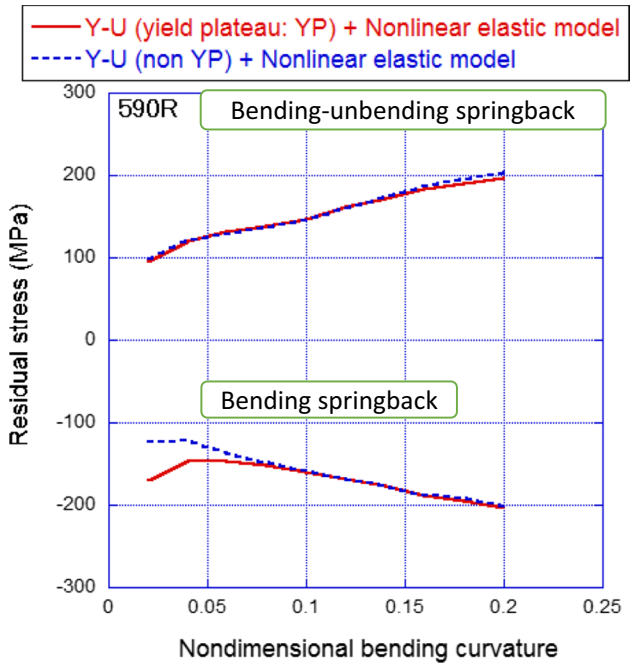

Fig. 24 Residual stresses of the 590R calculated by Y-U model with and without consideration of the YP when using nonlinear elastic model

plastic-strain-dependent elasticity models (two linear models of chord modulus and YSA modulus and the nonlinear elastic model) combined with two types of plasticity models (the Y-U pure-KH model and A-F + IH model) were exam-

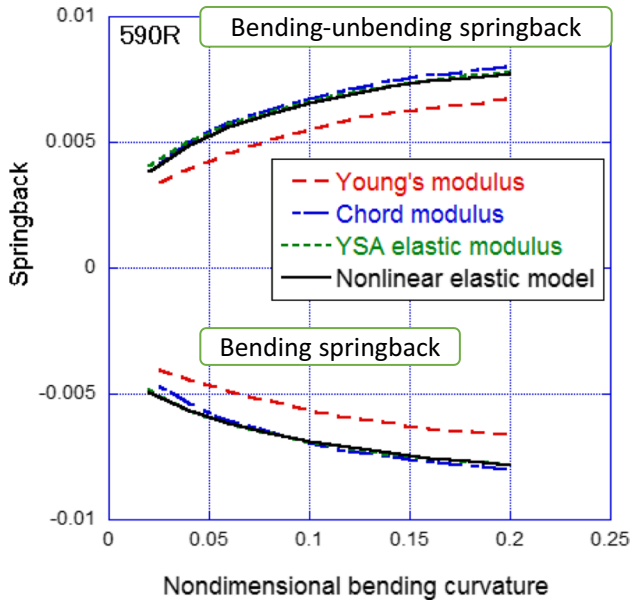

Fig. 25 Springback of the 590R calculated by the Y-U_YP model in combination with several types of elastic models

ined by performing cyclic stress–strain simulation and the

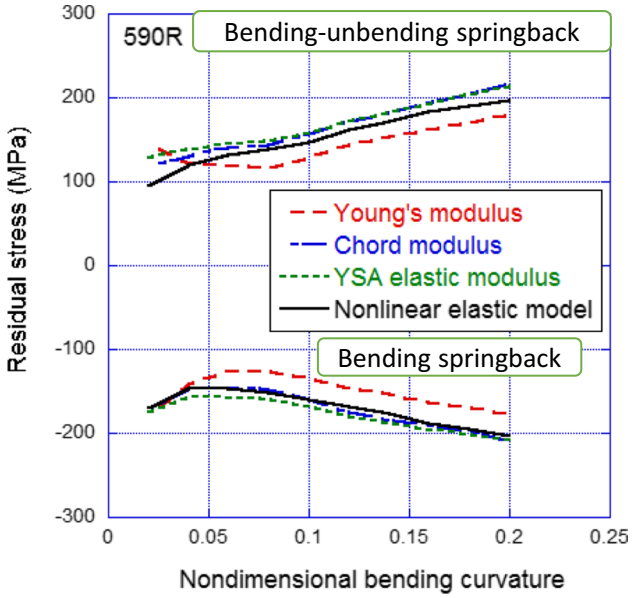

Fig. 26 Residual stresses in the 590R calculated by Y-U _YP model in combination with several types of elastic models

bending-unbending springback simulation for DP980 AHSS and 590R HSS sheets. The main findings and some remarks of this study are summarized as follows:

1. The best model to describe the smooth elastic–plastic transition behavior and realistic cyclic stress-strain responses was the Y-U model combined with the nonlinear elastic model. The elastic–plastic behaviors calculated by the Y-U with the linear elastic models were not very different from the results obtained by the nonlinear elastic model. Consequently, the calculation errors of springback and the residual stresses, when using the linear models, were less than 4% and 6%, respectively, compared with the nonlinear elastic model calculation. Therefore, the use of plastic-strain-dependent linear elastic models would be a good choice for industrial springback prediction because linear models have a great advantage over nonlinear models in terms of computational cost.
2. In contrast to the Y-U model, when using the A-F + IH model, the simulation results of the elastic–plastic transition behavior and springback, as well as residual stresses, were very different depending on the types of elastic models; for example, the errors of springback and residual stresses reach 7% and 14%, respectively. However, when using the nonlinear elastic model combined with the A-F + IH model, the calculated springback and residual stresses were close to the Y-U model predictions. Hence, it is concluded that when using the A-F

+ IH model, the use of the nonlinear elastic model is essential for springback analysis.

3. The effect of yield plateau on springback was limited only in small bending ($\overline{\kappa}_0 < 0.05$).

Appendix

Anisotropies and the plane-strain stresses of DP980 and 590R

The stress and r-value anisotropies in three sheet directions (0 °, 45 ° and 90° from the rolling direction) of the DP980 and 590R sheets are listed in Tables 5 and 6, respectively. For the equi-biaxial stress, $\sigma_x/\sigma_0 = \sigma_y/\sigma_0 = \sigma_b/\sigma_0 = 1.0$ was assumed after Yoshida et al. [37] for both sheets. Using these anisotropy properties, the material parameters of the following six-ordered polynomial (6-poly) type yield function [38], C_1~C_{16} were determined (see Tables 7 and 8 for DP980 and 590R, respectively):

$$\begin{aligned}&\phi = C_1\sigma_x^6 - 3C_2\sigma_x^5\sigma_y + 6C_3\sigma_x^4\sigma_y^2 - 7C_4\sigma_x^3\sigma_y^3 + 6C_5\sigma_x^2\sigma_y^4 - 3C_6\sigma_x\sigma_y^5 + C_7\sigma_y^6 \\ &+ 9\left(C_8\sigma_x^4 - 2C_9\sigma_x^3\sigma_y + 3C_{10}\sigma_x^2\sigma_y^2 - 2C_{11}\sigma_x\sigma_y^3 + C_{12}\sigma_y^4\right)\tau_{xy}^2 \\ &+ 27\left(C_{13}\sigma_x^2 - C_{14}\sigma_x\sigma_y + C_{15}\sigma_y^2\right)\tau_{xy}^4 + 27C_{16}\tau_{xy}^6 \\ &= \sigma_0^6.\end{aligned} \tag{36}$$

Table 5 Stress anisotropies of DP980 and 590R sheets determined from uniaxial tensions in three sheet directions (0 °, 45 ° and 90° from rolling direction)

	σ_0/σ_0	σ_{45}/σ_0	σ_{90}/σ_0
DP980	1.000	1.004	0.998
590R	1.000	0.972	1.033

Table 6 R-value anisotropies of DP980 and 590R sheets in three sheet directions

	r_0	r_{45}	r_{90}
DP980	0.82	0.80	0.82
590R	0.57	1.10	0.72

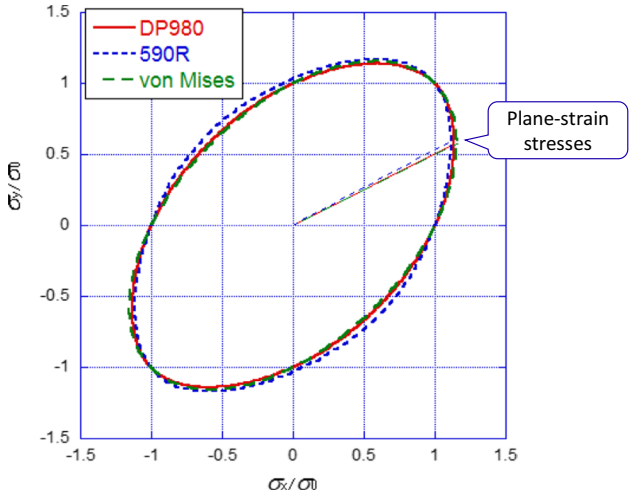

Fig. 27 Yield surfaces of DP980 and 590R calculated by the six-ordered polynomial yield function and von Mises yield function

Figure 27 shows the 6-poly yield surfaces for DP980 and 590R, as well as the von Mises yield surface.

The plane-strain stress components are determined from the following equation:

$$\begin{aligned}&\dot{\varepsilon}_y^p = \frac{\partial\phi}{\partial\sigma_y}\dot{\lambda} \\ &= \left(-3C_2\sigma_x^5 + 12C_3\sigma_x^4\sigma_y - 21C_4\sigma_x^3\sigma_y^2 + 24C_5\sigma_x^2\sigma_y^3 - 15C_6\sigma_x\sigma_y^4 + 6C_6\sigma_y^5\right)\dot{\lambda} \\ &= 0.\end{aligned} \tag{37}$$

The calculated results are $\sigma_x/\sigma_0 = 1.135$, $\sigma_y/\sigma_0 = 0.578$ for DP980, and $\sigma_x/\sigma_0 = 1.115$, $\sigma_y/\sigma_0 = 0.593$ for 590R, both of which are not very far from the von Mises calculation of $\sigma_x/\sigma_0 = 1.155$, $\sigma_y/\sigma_0 = 0.577$.

Table 7 Material parameters in the six-ordered polynomial yield function for DP980

C_1	C_2	C_3	C_4	C_5	C_6	C_7	C_8
1.0000	0.9011	0.8934	0.8961	0.8899	0.9120	1.0121	0.9587
C_9	C_{10}	C_{11}	C_{12}	C_{13}	C_{14}	C_{15}	C_{16}
0.8501	0.7783	0.8517	0.9666	0.9030	0.5574	0.9007	0.7453

Table 8 Material parameters in the six-ordered polynomial yield function for 590R

C_1	C_2	C_3	C_4	C_5	C_6	C_7	C_8
1.0000	0.7261	0.6212	0.5697	0.6138	0.6890	0.8230	0.9934
C_9	C_{10}	C_{11}	C_{12}	C_{13}	C_{14}	C_{15}	C_{16}
0.8042	0.7087	0.7910	0.9121	1.0334	0.7456	1.0479	1.1576

Acknowledgements The author would like thank Dr. Misao Itoh for his great help with the experiment.

Author's contribution This study was solely conducted by the present author.

Funding This study was supported by Hiroshima University and CEM Institute Corporation.

Declarations

Conflicts interests/competing interests The author declares that he has no conflict of interest or competing interest.

References

1. Cleveland RM, Ghosh AK (2002) Inelastic effects on springback in metals. Int J Plast 18:769–785
2. Yoshida F, Uemori T, Fujiwara K (2002a) Elastic-plastic behavior of steel sheets under in-plane cyclic tension-compression at large strain. Int J Plast 18:633–659
3. Yoshida F, Uemori T (2002b) A model of large-strain cyclic plasticity describing the Bauschinger effect and workhardening stagnation. Int J Plast 18:661–686
4. Geng L, Wagoner RH (2002) Role of plastic anisotropy and its evolution on springback. Int J Mech Sci 44:123–148
5. Yoshida F, Uemori T (2003) A model of large-strain cyclic plasticity and its application to springback simulation. Int J Mech Sci 45:1687–1702
6. Chung K, Lee MG, Kim D, Kim C, Wenner ML, Barlat F (2005) Spring-back evaluation of automotive sheets based on isotropic–kinematic hardening laws and non-quadratic anisotropic yield functions: Part I: Theory and formulation. Int J Plast 21:861–882
7. Fei D, Hodgson P (2006) Experimental and numerical studies of springback in air v-bending process for cold rolled TRIP steels. Nucl Eng Des 236:1847–1851
8. Lee MG, Kim D, Kim C, Wenner ML, Wagoner RH, Chung K (2007) A practical two-surface plasticity model and its application to springback prediction. Int J Plast 23:1189–1212
9. Yu HY (2009) Variation of elastic modulus during plastic deformation and its influence on springback. Mater Des 30:846–850
10. Zang SL, Liang J, Guo C (2007) A constitutive model for springback prediction in which the change of Young's modulus with plastic deformation is considered. Int J Mach Tools Manuf 47:1791–1797
11. Eggertsen P-A, Mattiasson K (2009) On the modelling of the bending-unbending behaviour for accurate springback predictions. Int J Mech Sci 51:547–563
12. Eggertsen P-A, Mattiasson K (2010) On constitutive modeling of springback analysis. Int J Mech Sci 52:804–818
13. Ghaei A, Green DE, Altenhof WJ (2009) Finite element simulation of springback for a channel draw process with drawbead using different hardening models. Int J Mech Sci 51:314–325
14. Ghaei A, Green DE, Aryanpour A (2015) Springback simulation of advanced high strength steels considering nonlinear elastic unloading-reloading behavior. Mater Des 88:461–470
15. Yilamu K, Hino R, Hamasaki H, Yoshifda F (2010) Air bending and springback of stainless steel clad aluminum sheet. J Mater Process Technol:272–278
16. Sun L, Wagoner RH (2011) Complex unloading behavior: nature of the deformation and its consistent constitutive representation. Int J Plast 27:1126–1144
17. Chatti S, Hermi N (2011) The effect of non-linear recovery on springback prediction. Comput Struct 89:1367–1377
18. Kim H, Kim C, Barlat F, Pavlina E, Lee MG (2013) Nonlinear elastic behaviors of low and high strength steels in unloading and reloading. Mater Sci Eng A 562:161–171
19. Wagoner RH, Lim H, Lee M-G (2013) Advanced issue in springback. Int J Plast 45:3–20
20. Hassan HUI, Traphoner H, Gunter A, Tekkaya AE (2016) Accurate springback in deep drawing using pre-strain based multiple cyclic stress–strain curves in finite element simulation. Int J Mech Sci 119:229–241
21. Sumikawa S, Ishiwatari A, Hiramoto., J. (2017) Improvement of springback prediction accuracy by considering nonlinear elastoplastic behavior after stress reversal. J Mater Process Technol 241:46–53
22. Min J, Guo N, Hou Y, Jiang K, Chen X, Carsley JE, Lin J (2021) Effect of tension-compression testing strategy on kinematic model calibration and springback simulation of advanced high strength steels. Int J Mater Form 14:435–448
23. Morestin F, Boivin M (1996) On the necessity of taking into account the variation in the Young modulus with plastic strain in elastic-plastic software. Nucl Eng Des 162:107–116
24. Yamaguchi K, Adachi H, Takakura N (1998) Effects of plastic strain and strain path on Young's modulus of sheet metals. Met Mater 4:420–425
25. Chatti S (2013) Modeling of the elastic modulus evolution in unloading-reloading stages. Int J Mater Form 6:93–101
26. Lee, J., Lee, J-Y., Balat F., Wagoner, H., Chung, K., Lee, M-G., 2013. Extension of quasi-plastic-elastic approach to incorporate complex plastic flow behavior – application to springback of advanced high-strength steels, Int J Plast 45, 140–159.
27. Lee, E-H., Stoughton, T. B., Yoon, J. W., 2017. A new strategy to describe nonlinear elastic and asymmetric plastic behaviors with one yield surface. Int J Plast 98, 217–238.
28. Lee, J-Y., Lee, M-G., Barlat, F., Bae, G. 2017. Piecewise linear approximation of nonlinear unloading-reloading behaviors using a multi-surface approach. Int J Plast 93, 112–136.
29. Mróz Z (1967) On the description of anisotropic work hardening. J Mech Phys Solids 15:163–175
30. Eggertsen P-A, Mattiasson K, Hertzman J (2011) A phenomenological model for the hysteresis behavior of metal sheet subjected to unloading/reloading cycles. Trans ASME J Manuf Sci Eng 133:1–16
31. Yoshida AT (2020) Model for description of nonlinear unloading-reloading stress-strain response with special reference to plastic-strain dependent chord modulus. Int J Plast 130:102708
32. Armstrong PJ, Frederick CO (1966) A mathematical representation of the multiaxial Bauschinger effect. GEGB report RD/B/N731. Berkley Nuclear Laboratories

33. Yoshida F, Hamasaki H, Uemori T (2015) Modeling of anisotropic hardening of sheet metals including descriptions the Bauschinger effect. Int J Plast 75:170–188
34. Chaboche JL, Rousselier G (1983) On the plastic and viscoplastic constitutive equations, Part I and II. Transactions of ASME. J Press Vessel Technol 105:153–164
35. Chaboche JL (1986) Time-independent constitutive theories for cyclic plasticity. Int J Plast 2:149–188
36. Yoshida F (2000) A constitutive model of cyclic plasticity. Int J Plast 24(16):359–380
37. Yoshida F, Kaneda Y, Yamamoto S (2008) A plasticity model describing yield-point phenomena of steels and its application to FE simulation of temper rolling. Int J Plast 24:1792–1818
38. Yoshida F, Hamasaki H, Uemori T (2013) A user-friendly 3D yield function to describe anisotropy of steel sheets. Int J Plast 45:119–139